Systematic calculation of threshold displacement energies: Case study in rutile

M. Robinson,[1,*] N. A. Marks,[1] K. R. Whittle,[2] and G. R. Lumpkin[2]
[1]*Nanochemistry Research Institute, Curtin University, GPO Box U1987, Perth WA 6845, Australia*
[2]*Australian Nuclear Science and Technology Organisation, Locked Bag 2001, Kirrawee DC NSW 2232, Australia*
(Received 10 November 2011; published 8 March 2012)

A generalized and systematic method of calculating threshold displacement energies (E_d) using molecular dynamics simulations has been developed and applied to rutile TiO_2. Statistically representative results have been achieved through fine sampling of impact energy and trajectory for each atomic species. Each impact trajectory is drawn from a uniform distribution of points on a unit sphere, along which, primary knock-on atoms (PKAs) with kinetic energies in the range of 20–200 eV were introduced into lattices equilibrated to 300 K. Various definitions of E_d are explored, with values presented as probabilities of defect formation. Results for the Ti PKA agree well with experimental data with a value of E_d at around 69 eV. Simulations of O PKAs contrast greatly with Ti PKAs, with displacements occurring at significantly lower energies, resulting in an O value of E_d at 19 eV. Analysis shows that replacement chains on the O sublattice are a common feature and play a significant role in governing defect formation in rutile.

DOI: 10.1103/PhysRevB.85.104105 PACS number(s): 61.72.Cc, 61.82.Ms, 61.80.Az, 31.15.xv

I. INTRODUCTION

The threshold displacement energy (E_d) is a fundamental quantity that is pivotal in defining the radiation tolerance of a material. Along with defect formation energies and the energy barriers associated with defect migration, E_d is used to gain an understanding of how radiation damage accumulates within a material. In short, E_d relates the kinetic energy from an incident particle or primary knock-on atom (PKA), to the number of defects created from the resultant collisions.

An initial use of the threshold displacement energy was in analytical models of radiation damage production, such as the Kinchin-Pease[1] model and its modification, the Norgett-Robinson-Torrens (NRT) model.[2] The latter of these states that the residual number of Frenkel pairs (N_f) generated from a primary impact with kinetic energy E_i, is given by $N_f = \kappa E_i/E_d$, for all nuclear-deposited energies above E_d/κ. Here κ is defined as the displacement efficiency and is found to be around 0.4 for the majority of materials. Although these models do not account for lattice effects such as recombination due to diffusion, they provide a valuable resource to estimate defect production.

One of the main explicit uses of E_d is in the stopping and range of ions in matter (SRIM),[3] a popular computer simulation program based on the binary collision approximation (BCA). The SRIM model determines the evolution of the ballistic phase of radiation events by solving classical scattering integrals dependent on the impact parameter, atomic number, mass, and velocities of the colliding ions. The energy imparted through each collision then determines the overall defect production, implantation depth, and sputtering yield. To accomplish this, SRIM requires a number of material-specific thresholds, including E_d. Within SRIM, E_d is defined as the minimum energy required to knock the PKA far enough away from its lattice site so that it will not immediately return, producing a vacancy and interstitial (Frenkel) pair. From this definition, it is clear that defect production is directly dependent on E_d, suggesting that reliable results hinge on ascertaining an accurate value of E_d.

This work introduces an extensive, systematic approach to calculating E_d using molecular dynamics simulation. A large ensemble of PKAs are incorporated in which directions are drawn from a dense sampling of the unit sphere and kinetic energies are finely spaced. The methodology presented is utilized in a study of rutile TiO_2, where results can be compared to both experimental and simulation work. The statistically significant results achieved not only allow for a quantitative value of E_d but also enable in-depth analysis of the associated defect production mechanisms.

II. BACKGROUND

A. Determining the threshold displacement energy E_d

Although E_d is an important quantity, its exact definition varies dependent on its intended use. For instance, the definition used in SRIM presumes that displacement of the PKA leads directly to the formation of a stable Frenkel pair. However, dynamical effects allow for the possibility that the PKA is displaced from its lattice, yet no defects are formed. Accordingly, a more natural definition would be that E_d is the minimum energy required to produce a permanent defect or Frenkel pair, which may or may not involve displacement of the PKA. This subtlety is not supported within SRIM where lattice effects are not accounted for. In multicomponent systems, E_d may also be defined as the minimum energy required to produce a defect on the same sublattice as the PKA. This again raises issues, as multiple defects or defect clusters may involve atoms of different species.

Aside from its subjective definition, the measurement of E_d involves a number of elements that are open to variability. For example, E_d may be calculated as a weighted average across certain PKA directions or averaged across a whole set of directions. In the former case, it is impossible to know if the PKA directions sampled are representative of all possible directions and if the weightings assigned based on multiplicity are valid. In the latter case, gaining a representative set of directions may prove difficult and experimental studies tend to report E_d along principle crystal directions. Another critical

variable in the definition of E_d is the time scale on which defects are classified as stable. It is well known that over long time scales the recombination of Frenkel pairs through point defect diffusion reduces the number of residual defects after the initial impact. At the other end of the spectrum is the short time scale of the ballistic phase, where the kinetic energy of the PKA is transferred to lattice atoms, causing localized heating and creating multiple transient defects. The time scale for defining E_d is therefore bound by the initial few picoseconds of the impact event and the much longer times associated with diffusion processes. As E_d is defined as a threshold, the time scale is commonly taken as the end of the ballistic phase, which is material dependent but is normally of the order of tens of picoseconds. This time scale is not a problem for models of atomic collisions but is difficult to access via experimentation.

1. Determination by experiment

The complexities involved in defining E_d make the interpretation of experimental results difficult. The primary task faced by any experimental procedure is the ability to detect the onset of defect production. Creating displacements within the lattice is readily achievable using various methods of bombardment, commonly high-energy electron beam irradiation. The difficulties arise from the required level of precision and control of both the incident beam energy and the measuring apparatus for the simultaneous creation and detection of atomic displacements. Any measurements that are not carried out *in situ* will be subject to thermally driven recombination of Frenkel pairs, increasing the observed value of E_d.

Early experimental methods used to measure E_d were dependent on observable defect structures such as dislocations and were captured using techniques such as transmission electron microscopy (TEM). A good example of this approach is the work by Pells *et al.*[4,5] who used a high-voltage electron microscope (HVEM) as both the source of high-energy electrons and the damage monitoring device when in transmission mode. Their work studying α-Al_2O_3 was followed by a succession of studies in other oxides where values of E_d were compared to other experimental techniques.[6–8] It is clear that using TEM as the indicator of damage does not result in the exact threshold displacement energy. This is a consequence of the observable defect structures required for detection only occurring after the creation of a saturation of point defects. Although advances in high-resolution TEM may allow the detection of individual displacements or smaller defect structures, its application to the determination of E_d is very challenging.

An alternative approach to experimentally deriving E_d takes advantage of the optical properties of vacancies in oxide ceramics. By examining the absorption spectra of crystals irradiated with electrons of increasing energy, the point at which vacancies are formed can be determined. This technique, however, only allows the determination of E_d for anion PKAs, where trapping of electrons in anion vacancies creates F^+ and F centers (one electron and two electron capture, respectively), which absorb wavelength specific photons. Early work by Chen *et al.*[9] employed optical absorption techniques to calculate E_d for O in MgO, yielding a value around 60 eV, although this was noted to be an upper limit.

A more recent experimental procedure based on similar principles is time-resolved cathodoluminescence spectroscopy (TRCS). The onset of vacancy production in TRCS is determined by the detection of characteristic photons emitted from the decay of excited F-center states. The time dependency of the intensity of emitted photons can also be established to investigate the transient nature of the detected defects. TRCS has been employed by numerous groups to study various oxides, from CaO[10] to more complex titanates and zirconates.[11–13]

Values of E_d can also be ascertained experimentally through changes in electrical conductivity during electron bombardment. Monitoring the charge carrier removal rate as a function of incident electron energy gives an indication of E_d. Work by Meese *et al.*[14] used this approach to investigate ZnO, generating values for the O PKA at around 57 eV.

A review of experimental procedures for measuring E_d in a wide range of ceramics was produced by Zinkle and Kinoshita in 1997.[15] This work consolidates results from previous reports into a table of recommended values of E_d for each ceramic. Values for the O PKA ranged from 20 to 60 eV.

2. Determination by simulation

The introduction of molecular dynamics (MD) computer simulation has allowed in-depth studies into all areas of radiation damage, including the calculation of threshold displacement energies. The ability to evolve large systems of particles at the atomistic level has allowed insights into defect production mechanisms. This insight is key to understanding how initial defects are formed and aids the calculation and interpretation of E_d.

Early MD investigations into the dynamics of radiation damage were conducted by Gibson *et al.*[16] and Erginsoy *et al.*[17] These studies into α-iron were a step into modeling collisions using computational methods and focused on the mechanisms of initial defect formation, ascertaining values of E_d. Although these works were limited by computer power to small systems and relatively simple models, they gave insight to collision processes such as replacement chains and focused collision sequences. The work of Erginsoy *et al.* also discussed the idea of displacement probability, indicating that past the threshold displacement energy, defect formation is not guaranteed and along some PKA directions can be highly erratic. The work of Chadderton and Torrens on alkali halides soon followed,[18–20] allowing insights into the effect of a second atomic species on collision mechanisms. This work paid particular attention to focused collision sequences and channelling events, two significant mechanisms that impact upon defect formation.

More recently, advances in computational power and the introduction of parallelized MD implementations has enabled statistically significant studies to take place that have involved more sophisticated models. A succession of MD studies into SiC by Malerba and Perlado *et al.*[21–23] indicated the difficulties of ascertaining a single value for E_d. Upper and lower bounds were introduced, which marked a range of PKA energies where defect formation is probabilistic. This work also examined the effect of temperature on initial defect formation and noted minimal effect on the value of E_d. A recent extensive MD investigation into Fe by Nordlund *et al.*,[24] investigated

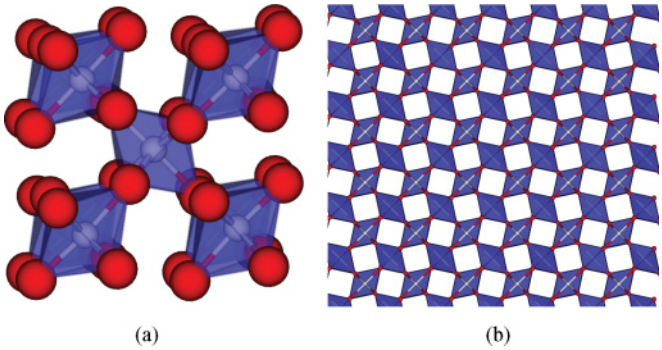

FIG. 1. (Color online) The crystal structure of rutile TiO_2 (TiO_6 octahedra are shown in blue). (a) extended unit cell (b) ⟨110⟩ plane highlighting the connectivity of the TiO_6 octahedra.

the dependency of E_d on the interatomic potential used. This comprehensive study involved a large number of PKA directions for each potential tested, allowing statistically sound comparisons. The significant number of statistics also allowed accurate definition of defect formation probability as a function of PKA energy. A large variation in E_d was reported between potentials, yet the trends found in simulation correlated well with experiment. This work also highlighted the difficulties in defining E_d and demonstrated various ways of determining a value.

B. Rutile TiO_2

TiO_2 is a heavily studied oxide with applications in a wide range of areas including photovoltaics, photocatalysis, and chemical sensing.[25–28] In addition to these uses, the rutile polymorph of TiO_2 in ceramic form is of considerable interest as a nuclear material, due to its presence in Synroc-type waste forms. Furthermore, the structure of rutile bares close similarities to numerous other radiation-tolerant ceramics, yet is itself a relatively simple structure. The chains of TiO_6 octahedra that make up the crystal (see Fig. 1) relate well to other polyhedra that are the building blocks in fluorite derivatives such as pyrochlore ($A_2B_2O_7$) or spinels (AB_2O_4). Therefore, understanding mechanisms of defect production in rutile may give a general insight to more complex materials.

An early experimental study into determining E_d for rutile was carried out by Buck.[29] This study was motivated by the development of Synroc and the interest of rutile to the nuclear community. The experimental procedure employed HVEM and TEM to study the effects of electron irradiation on defect formation. Observations of damage development related to an E_d value of between 45 to 50 eV for Ti. Although damage was observed that would correspond to an O value of around 33 eV, the damage could not be solely attributed to O displacements. This work also indicated that the radiation response of rutile was consistent with that of other oxide ceramics.

A series of studies by Smith *et al.* used TRCS to measure O E_d values for rutile along with various other titanates and zirconates.[11–13,30] This work found a remarkably consistent value of E_d for O PKAs across all the oxides considered at around 40–50 eV, with the rutile value at 39 ± 4 eV. Results correlated well with experimental work and through the comparison of the different oxide structures, suggested that E_d is correlated to the coordination of the O site.

Initial MD computer simulations to determine E_d in rutile TiO_2 were carried out by Richardson.[31] Rutile was found to be highly anisotropic in relation to PKA trajectory, resulting in difficulties in defining a single value E_d. This work also reported how defects on the O sublattice would be a prominent feature for both Ti and O PKA simulations. Ti PKAs were reported to have a higher value of E_d around 50 eV, with O PKAs much lower and highly variable, anywhere between 10 and 40 eV.

A more recent computational study of E_d in rutile was carried out by Thomas *et al.*[32] This study also calculated defect formation energies. It involved extensive calculations of E_d along principle lattice directions, with the final value taken as a weighted average. Using a similar idea to Nordlund *et al.*[24] and Malerba *et al.*,[23] E_d was defined as a function of defect formation probability (DFP) and taking a DFP of 10% gave values of E_d at 40 eV and 105 eV for O and Ti PKAs, respectively. However, this work indicated the sporadic nature of the DFP as a function of PKA energy along single directions and emphasised the need for good statistics. Values of E_d correlated well with the work of Richardson[31] and previous experimental findings, although the value of E_d for Ti was found to be higher than reported by Buck.[29]

III. METHODOLOGY

This work determines E_d through a large number of low-energy MD collision cascades carried out using the DL_POLY code.[33] Equilibrium interactions are based on the Matsui-Akaogi (MA) pair potential $\phi_{MA}(r_{ij})$,[34]

$$\phi_{MA}(r_{ij}) = A\exp\left(\frac{-r_{ij}}{\rho}\right) - \frac{C}{r_{ij}^6}, \quad (1)$$

which has had numerous successes in modeling rutile TiO_2. To correctly depict close-range interactions of nuclei that frequently occur during collision simulations, modifications to the MA pair potentials are required. At small atomic separation, the highly repulsive Coulomb forces from the nuclei can be accurately modeled by the Ziegler-Biersack-Littmark pair potential $\phi_{ZBL}(r_{ij})$.[35] With accurate representations of both equilibrium and short-range interactions, there is a contrasting lack of protocol when defining the intermediate region. It is clear that the transition from one potential to another should be smooth through to the second derivatives to ensure conservation of energy during the MD simulations. In addition, the transition region should be as short as possible and occur far from the equilibrium interaction range to maintain the correct representation of bulk properties. Apart from these constraints, other properties of the transition region such as its functional form and the exact interaction range are somewhat arbitrary. For simulations of high-energy collisions, slight variations in defining this region may not have a significant effect on overall findings. However, as Nordlund *et al.*[24] discuss, this region directly impacts the value of E_d due to the lower-energy collisions involved. It is therefore vital that care be taken when defining the transition region and during the fitting process.

We follow an approach employed by Smith *et al.*[36,37] which uses an exponential function of the form

$$\phi_S(r_{ij}) = e^{a_0+a_1 r_{ij}+a_2 r_{ij}^2+a_3 r_{ij}^3+a_4 r_{ij}^4+a_5 r_{ij}^5}, \quad (2)$$

where the parameters a_i are found by fitting the function, its derivative and second derivative of the close-range and equilibrium potentials at two points r_a and r_b. The values of r_a and r_b are chosen to produce a smooth transition region with the constraints that $r_{(b)}$ lies sufficiently far from the equilibrium atomic separation and the transition region itself is minimal. Using a function of this form allows a smoother fit than other cubic polynomials. A minor issue with using an exponential form is the inability to fit to a region that is negative, although this can be easily circumvented by adding a constant during the fitting process.

For the pair potentials used in this work, the functional form shown in Eq. (2) was found to be sufficiently smooth, resulting in the overall pair potential,

$$\phi(r_{ij}) = \begin{cases} \phi_{\mathrm{ZBL}}(r_{ij}) & \text{if} \quad r_{ij} < r_a \\ \phi_S(r_{ij}) & \text{if} \quad r_a \leqslant r_{ij} \leqslant r_b \\ \phi_{\mathrm{MA}}(r_{ij}) + \phi_{\mathrm{elec}}(r_{ij}) & \text{if} \quad r_{ij} > r_b. \end{cases}$$

Simulations employ fixed partial charges of −1.098 and 2.196 for O and Ti respectively, with the long-range electrostatic contributions $\phi_{\mathrm{elec}}(r_{ij})$ summed using the Ewald method. It is important to note that the Ewald summation includes the electrostatic contribution from all pairs of atoms regardless of the separation. Therefore, if the separation of a pair of atoms is less than r_b, the electrostatic contribution must be subtracted from the overall potential to ensure that the potential is solely attributed to $\phi_{\mathrm{ZBL}}(r_{ij})$ or $\phi_S(r_{ij})$. This can be achieved either during the simulation or, as in the case of this work, during the fitting process. For the Ti-Ti and Ti-O potentials, the electrostatic contribution, ϕ_{elec}, was subtracted from ϕ_{ZBL} potential before the fitting to the MA potential ϕ_{MA}. For the O-O potential, a smoother fit was achieved by first adding ϕ_{elec} to ϕ_{MA} before fitting to ϕ_{ZBL}. In this case, ϕ_{elec} was subtracted from the complete interaction range after fitting. The fitting parameters and potential parameters are provided in Table I.

During the fitting procedure it became clear that the O-O interaction generated by ϕ_{MA} was considerably more repulsive than the potential given by ϕ_{ZBL} at small atomic separation. This unrealistic behavior can potentially cause issues with the fitting procedure. For this reason, the transition region from ϕ_{MA} to ϕ_{ZBL} had to start closer to the O-O equilibrium bond length than the Ti-O and Ti-Ti interactions, before the potential became too repulsive.

TABLE I. Potential parameters and fitting parameters used in the MD simulations.

	Ti-O	Ti-Ti	O-O
a_0	11.43859369	10.47821944	9.143828241
a_1	−19.02695742	−5.750211430	−10.86376623
a_2	25.16633969	−16.11160003	7.308749502
a_3	−19.12969787	41.22109905	−2.394044113
a_4	6.598933976	−38.27252655	0.2996524487
a_5	−0.8589593073	12.16901160	−0.2763183665e-4
r_a	0.6	0.4	0.4
r_b	1.6	1.0	2.4
A	16957.53	31120.20	11782.76
ρ	0.1940	0.154	0.234
C	12.59	5.25	30.22

A. Determining primary knock-on atom directions

The determination of E_d depends on the transition region between a stable lattice and the onset of defect formation as PKA energy increases. If this region is discrete then various search algorithms can be utilized, such as the bisection search algorithm.[38] This speeds up calculation of E_d and allows more time for an increase in sampling variables such as PKA direction. However, as detailed in numerous works including those by Nordlund *et al.*[24] and Malerba *et al.*,[23] in many materials the energy at which defect formation occurs is indistinct, which introduces a notion of defect formation probability. Therefore, to accurately determine the defect formation probability as a function of PKA energy, which will allow E_d to be extrapolated, an extensive systematic approach is adopted. This involves statistically robust sampling of PKA energy, direction, and initial thermal motion for each PKA species.

Traditionally, methods of sampling PKA directions take advantage of the symmetry present in the crystal under study.[24,37,39] This involves constructing an irreducible volume from which directions are drawn. However, as the complexity of the crystal structure increases, the task of determining the set of symmetry-unique directions and achieving uniform sampling becomes highly challenging. Additionally, for crystals at finite temperature the instantaneous symmetry is broken due to atomic motion. The breaking of symmetry is extremely important in the evolution of the PKA event due to the branching and chaotic nature of the collisions.

To enable a procedure for calculating E_d that can be used for complex crystal types, the method of determining PKA directions needs to be generalized. The most intuitive way of accomplishing this is to uniformly sample across the surface of a sphere. If this sampling is fine enough, it will allow for direct averaging over all directions to generate the value of E_d. However, uniformly distributing a large amount of points on the surface of a sphere is a nontrivial task, with no analytical solution. In fact, this problem is of historical significance, as it was initially outlined by Thomson in 1904 whilst attempting to determine the arrangement of point charges in the atom.[40,41] The Thomson problem, as it now referred to, has since been generalized into finding the minimum energy configuration of N point charges on a sphere and has formed a significant area of research, applicable to a multitude of real-world problems from the structure of fullerenes to morphology of viruses. The need for numerical procedures to determine minimum energy configurations is well documented[42–46] along with values of the minimum energy for $N<100$. For large N, the number of local minima increases exponentially and finding the global minimum using simple numerical algorithms becomes a time-consuming task. More recent Monte Carlo techniques by Perez-Garrido *et al.*,[47–49] who discuss the importance of dislocations in the lattice have had success in defining minimum energy configurations for larger systems. Significant work has also been carried out by Wales *et al.*[50–53] who

employed a basin-hopping minimization method.[54] Using this methodology, Wales has systematically reported minimum energy structures for $N < 400$, with selected structures up to $N = 4352$.[55]

In this work, PKA trajectories were generated by sampling from a unit sphere obtained by solving the Thomson problem with the number of points $N = 100$. A molecular dynamics (MD) minimization technique, separate from the main MD simulations, was adopted incorporating the velocity Verlet algorithm, with each point given unit mass and the time step set to a nominally small value. Using MD allows the control of temperature through velocity scaling, which can help the system escape out of local minima. Although finding the global minimum to solve the Thomson problem for large N requires more advanced minimization techniques, for the purposes of this work MD is more than sufficient.

The effective force $\mathbf{F}_{\text{eff}}$ used during minimization is given by the Coulomb force, $\mathbf{F}_i^{\text{True}}$, with the radial component removed,

$$\mathbf{F}_i^{\text{Eff}} = \mathbf{F}_i^{\text{True}} - \left(\mathbf{F}_i^{\text{True}} \cdot \hat{\mathbf{r}}_i\right)\hat{\mathbf{r}}_i, \tag{3}$$

where

$$\mathbf{F}_i^{\text{True}} = -\nabla\phi_i(\mathbf{r}_1, \mathbf{r}_2, \ldots, \mathbf{r}_n), \tag{4}$$

$$\phi_i(\mathbf{r}_1, \mathbf{r}_2, \ldots, \mathbf{r}_n) = \sum_{i \neq j} \frac{1}{r_{ij}}, \tag{5}$$

$$r_{ij} = |\mathbf{r}_i - \mathbf{r}_j|. \tag{6}$$

Removing the radial component of $\mathbf{F}_i^{\text{True}}$ results in $\mathbf{F}_i^{\text{Eff}}$ being tangential to the surface of the sphere. To ensure each point remains on the surface the positions are renormalized to the surface at each simulation step using

$$\hat{\mathbf{r}}_\mathbf{i} = \frac{\mathbf{r}_i}{|\mathbf{r}_i|}. \tag{7}$$

The initial random configuration of 100 points on the unit sphere is shown in Fig. 2(a), with the final configuration post minimization shown in Fig. 2 (b). The minimized configuration indicated an hexagonal packing structure as highlighted by the radial distribution function in Fig. 2(c). The minimized energy agreed well with the value reported elsewhere.[45,46,55] An example of how these points will represent PKA directions in shown in Fig. 3 for the Ti PKA.

B. Defect analysis

Due to the significant amount of data generated from the collision cascade MD simulations, postsimulation analysis through visualization of each individual simulation was impossible. Therefore, there was a need for thorough on-the-fly analysis, which takes place at the end of each simulation. To ensure all important quantities were recorded, numerous analysis algorithms were employed.

First, all vacancies, interstitial, and replacement defects were determined. The defects are then classified into regions, to make categorization of defect clusters easier and to also indicate regions of localized damage. The separation of Frenkel pairs (FPs) was also recorded to determine if the changes in PKA species result in different distributions of defects. When multiple vacancies and interstitials are created,

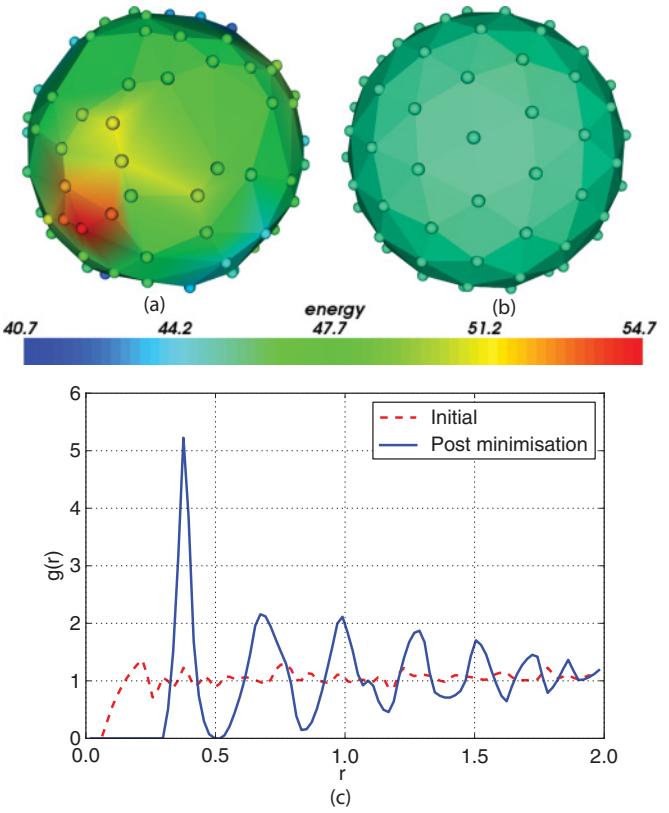

FIG. 2. (Color online) The PKA impact directions taken from a solution to the Thomson problem for $N = 100$. (a) Initial randomized configuration. (b) MD relaxed configuration. (c) The initial (dashed) and relaxed (solid) radial distribution functions.

separations are calculated by systematically pairing up the closest FP of the same species. An important quantity to study is the creation of replacement chains resulting from focused collision sequences. The existence of these mechanisms is well known[16,17] and can help dissipate the impact energy of the PKA. The creation of replacement chains can also aid damage recovery if loops are formed. Analysis included the calculation of both replacement chains and loops, with the length of each loop categorized by the number of atoms involved. For example, a replacement loop of length 2 is a simple nearest neighbor exchange. The defect analysis is

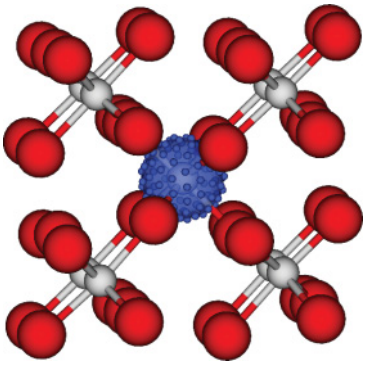

FIG. 3. (Color online) The points on the blue sphere indicate one hundred PKA impact directions for the Ti PKA taken from the solution to the Thomson problem.

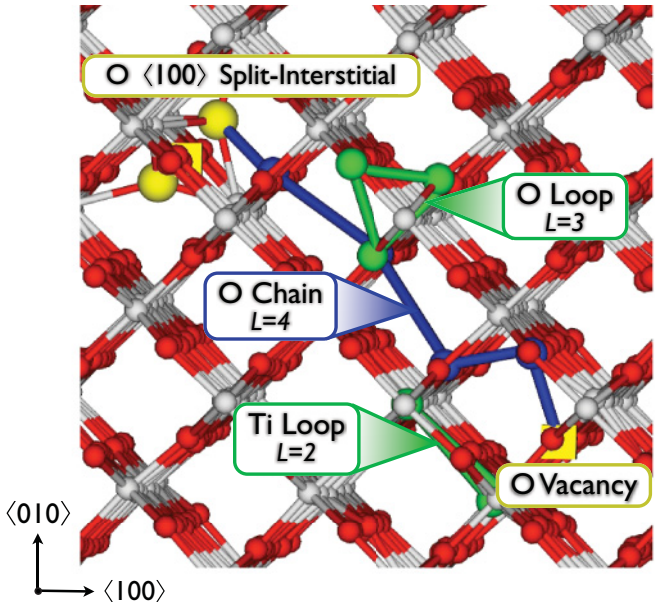

FIG. 4. (Color online) Illustration of the replacement chains and loops formed during the MD simulations. The configuration shown was the result of a 175 eV cascade simulation initiated by a Ti PKA. L indicates the number of atoms involved in the chain or loop (i.e., the Ti loop where $L = 2$) is a simple nearest neighbor replacement and is found consistently during the simulations.

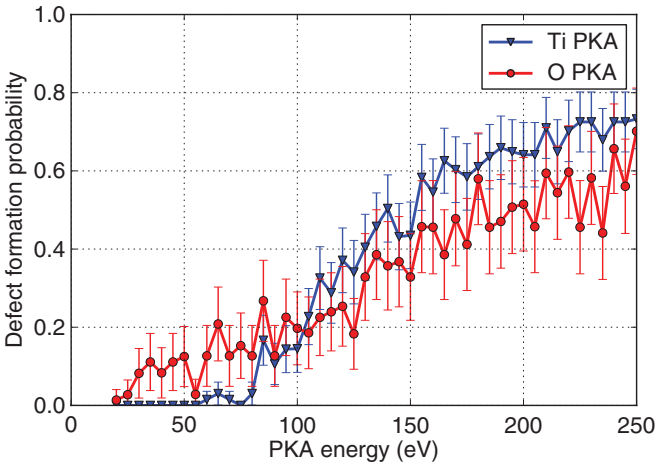

FIG. 5. (Color online) Defect formation probability for both Ti and O PKA averaged across main crystallographic PKA directions at 160 K. Error bars represent a 95 % confidence interval of the standard error in the mean (SEM).

demonstrated in Fig. 4, which contains both replacement chains and loops, highlighting example mechanisms for the production and recombination of point defects.

C. Computational procedure

Before the collision cascades take place, a set of 10 rutile lattices were created and equilibrated to 300 K using the Nosé-Hoover thermostat.[56] After initial testing of system sizes, a supercell of 4608 atoms (8×8×12 unit cells) was found to be sufficiently large to contain the cascades. Periodic boundary conditions were employed in each of the Cartesian directions along with a 3.5Å thermal layer for removing the kinetic energy introduced by the PKA. Equilibration times were varied between 12 and 20 ps to allow for changes in thermal motion. In each lattice a PKA was chosen near to the center of the cell and given a kinetic energy in range of $20 \leqslant E < 200$ eV at increments of 5 eV. At each energy, MD collision cascade simulations were initiated along the one hundred PKA directions as sampled from the unit sphere. The system was then evolved in the traditional MD manner for 10 ps, which is more than sufficient to capture the ballistic phase of the cascade. After completion of the defect analysis described above the redundant MD data was disregarded. This procedure was carried out for both atomic specie, resulting in 72000 MD simulations.

IV. RESULTS

A. Simulations at 160 K

In previous work by Thomas *et al.*,[32] simulations were carried out at 160 K using only principle crystallographic directions and five different lattices. To make direct comparisons, the same setup was employed in this work before the main set of simulations at 300 K. This also allowed insight into the effect of sampling points across a whole sphere in contrast to the main crystallographic directions.

Defect formation probability as a function of PKA energy for the simulations using only principle crystallographic directions is shown in Fig. 5. The uncertainty in the data makes extrapolation of values of E_d difficult, particularly for the O PKA. This was also noted by Thomas *et al.*, who reported a weighted average of 40 eV for O and 105 eV for Ti at 10% DFP. From Fig. 5, at 10% DFP, values of E_d would range from 60 ± 30 eV for O and 90 ± 10 eV for Ti. Although the error for the O PKA is quite large, the ranges correlate well with the results of Thomas *et al.* A significant difference in comparison to Thomas *et al.* is the quoted values for O at 50% DFP, at 65 eV. Simulations presented here suggest a value between 135 and 205 eV, a much higher range. In contrast, the Ti value published by Thomas *et al.* for 50% DFP was 130 eV, which agrees well with the value calculated here of between 135 and 150 eV. A reason for the observed difference in O DFP as PKA energy increases is the way in which the average DFP is calculated. In the work of Thomas *et al.* a Fermi function is fitted to DFP for each PKA direction. The values at 10 and 50% DFP are then interpolated from this fit. In the present work, at each energy the average is calculated over all directions. We adopted this approach due to the highly sporadic nature of DFP as a function of PKA energy for single directions, as shown in Fig. 6 for the ⟨100⟩ direction. The degree of irregularity is higher for O, with a more discrete threshold observed for the Ti PKA. This relates well to the differences with the work of Thomas *et al.*, where a Fermi function fit to the Ti data would be appropriate. The contrasting behavior of DFP as a function of PKA energy between each PKA species suggests differences in the mechanisms for defect production between collisions with Ti and O PKAs. An explanation of these mechanisms along with further analysis will be discussed during the main body of simulations, where results are supported by enhanced statistics.

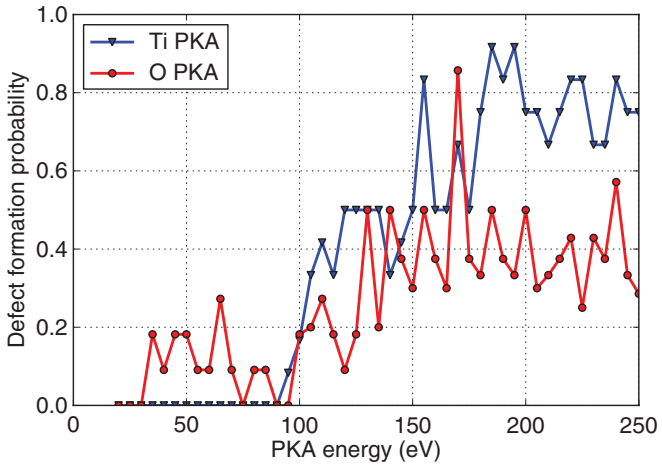

FIG. 6. (Color online) Defect formation probability for each PKA specie along the ⟨100⟩ direction at 160 K.

B. Simulations at 300 K

Results from simulations incorporating the full set of one hundred PKA directions as sampled on the unit sphere are presented here, with simulations carried out as described in the methodology section. The first quantity examined is the DFP as a function of PKA energy and can be found in Fig. 7. The first striking feature is the smoothness of both curves along with the high degree of precision achieved, as indicated quantitatively by the narrow 95% confidence interval. This is a distinct improvement over the preliminary study at 160 K (Fig. 5), which used around 2000 MD simulations. This indicates that the extensive degree of sampling implemented is a requirement for determining E_d. The dependency of DFP on PKA energy as shown in Fig. 7 supports the differences in values of E_d between the O and Ti PKA reported by Thomas *et al.*[32] and Richardson,[31] with the O PKA requiring significantly less

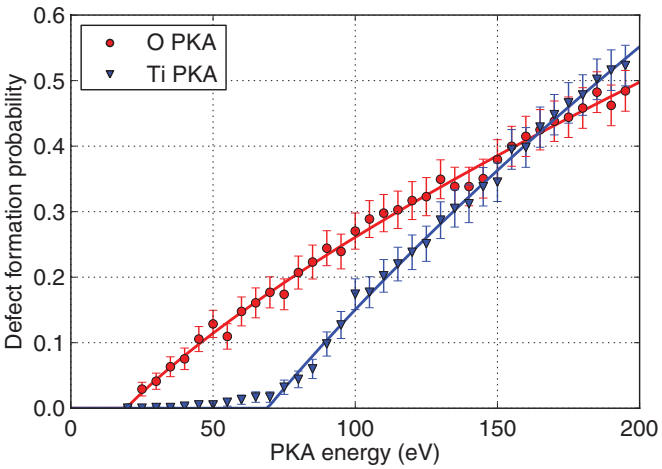

FIG. 7. (Color online) Defect formation probabilities (DFPs) for both Ti and O PKA averaged across all 100 PKA directions. Each point represents 1000 MD simulations, with each direction carried out in 10 different lattices equilibrated to 300 K. Error bars represent a 95% confidence interval of the SEM. The solid line represents the piecewise power-law fit of DFP against PKA energy [Eq. (8)]. Values of E_d at 0% DFP are 19.4 and 69.1 eV for O and Ti respectively.

energy to initiate defect formation. Using the approach of Thomas *et al.*, it is simple to extract energies at which the DFP is 10%, resulting in 45 eV for O and 90 eV for Ti. Although these values agree well with the work of Thomas *et al.* and experimental values of E_d for O,[11,29] the physical reasoning for relating E_d to a 10% DFP is somewhat arbitrary.

For a more mathematical approach to defining E_d and as there is a significant amount of data gathered, it is sensible to define an expression for the dependency of DFP on PKA energy. Ideally, the functional form should intersect at 0% DFP to define a value of E_d and also converge to 100% DFP in a sensible manner. However, after fitting various functions based on exponential and sigmoidal forms, it became clear that a single function could not fit the data precisely around E_d and also converge slowly to DFP = 100%. As it is more important to accurately fit the data around E_d, a simple piecewise power law was chosen that was found to fit the data from both the O and Ti PKA closely:

$$\mathrm{DFP}(E) = \begin{cases} 0 & \text{if} \quad E \leqslant E_d \\ \frac{1}{\beta}[E^{\alpha} - (E_d)^{\alpha}] & \text{if} \quad E > E_d \end{cases} \tag{8}$$

where α and β are fitting parameters and E is the energy of the PKA. This function allows the intersect at E_d to vary during the fitting process.

The resultant fit is shown in Fig. 7 and generates O values of 19.4 eV, 0.692 and 62.8 and Ti values of 69.1 eV, 0.652 and 28.6 for E_d, α, and β respectively. The value of E_d for oxygen at 19.4 eV is significantly lower than experimentally reported values of around 40 eV.[11,29] There is a much better agreement for the Ti value of E_d at 69.1 eV to both experimental and simulation work.[29,31,32] Rearranging Eq. (8) and inserting a DFP of 0.1 results in energies of 45.7 eV for O and 89.2 eV for Ti, close to the values extrapolated previously. What is apparent from Fig. 7 is the broad range of energies over which defect formation is probabilistic. This range is large for O in comparison to Ti, as indicated by the lower value of E_d yet the higher energy required to give a DFP of above 50%. As a result, a crossover between Ti and O at around 160 eV is created at which point it becomes more likely to form a defect by displacing a Ti than O. The difference in the rate of increase in DFP as the PKA energy increases suggests different mechanisms for defect formation dependent on the species involved in the displacements. These mechanisms cannot simply be attributed to the mass differences between the Ti and O and shows that more complex lattice effects are taking place.

C. Implications for SRIM

In SRIM, E_d is defined as the minimum energy required to knock the PKA far enough away from its lattice site so that it will not immediately return. The assumption within SRIM is that this process produces a vacancy and interstitial (Frenkel) pair. This definition suggests a direct dependence of defect production on PKA displacement. To investigate this assumption, we defined an alternative probability dependent on whether the PKA remains in its original site. The resultant dependency of this PKA displacement probability on PKA energy can be found in Fig. 8, which also includes the previously calculated DFP. There are marked differences between

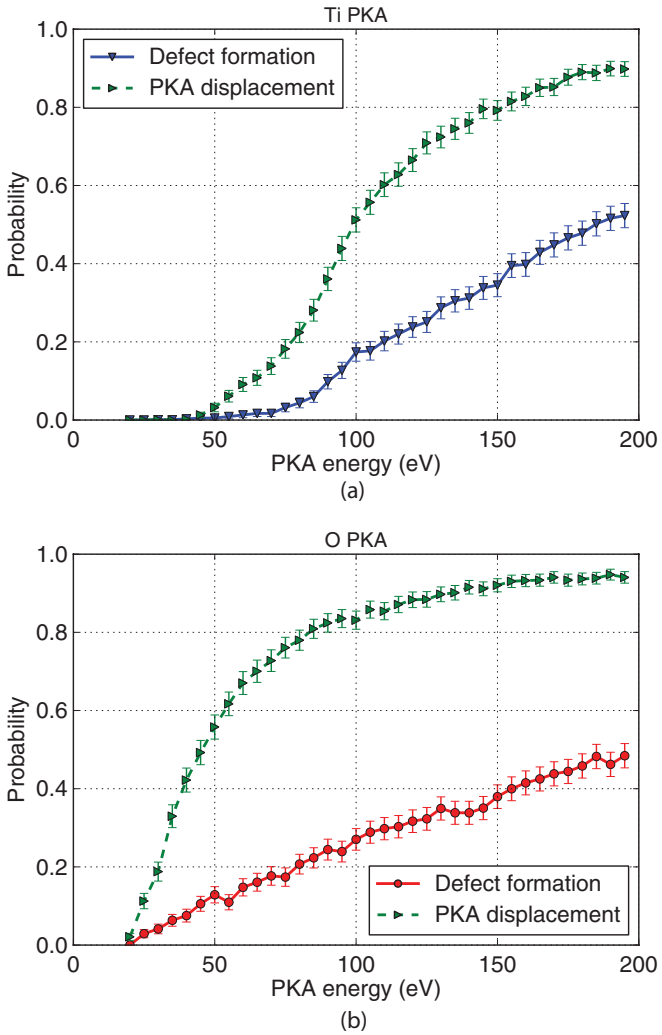

FIG. 8. (Color online) Probabilities of PKA displacement and defect formation for the (a) O PKA and (b) Ti PKA as a function of PKA energy.

the PKA displacement probability and the DFP both generally and through its dependency on PKA species. First, there is a much more discrete threshold for PKA displacement, with the probability rising sharply once this threshold is met to around 90% at 200 eV for both PKAs. This may be as expected as once the PKA energy is sufficiently higher than the binding energies associated with the PKA to its site, the PKA will be displaced. What is interesting is the observed difference in the probability of PKA displacement in comparison to defect formation. For the O PKA the difference is significant, for example at 100 eV, whilst there is around 80% probability of displacing the O atom, there is only a 30% probability of creating a stable Frenkel pair. Although the atomic displacements are correlated to the formation of stable defects, this suggests there exists a saturation point before which displacements and replacements dissipate the impact kinetic energy, counteracting defect formation. This idea suggests that in materials susceptible to amorphization, these mechanisms of recovery cannot be accessed and PKA displacement would correlate more strongly with defect formation. The definition of E_d for these materials would be unambiguous, and would support its use in SRIM,

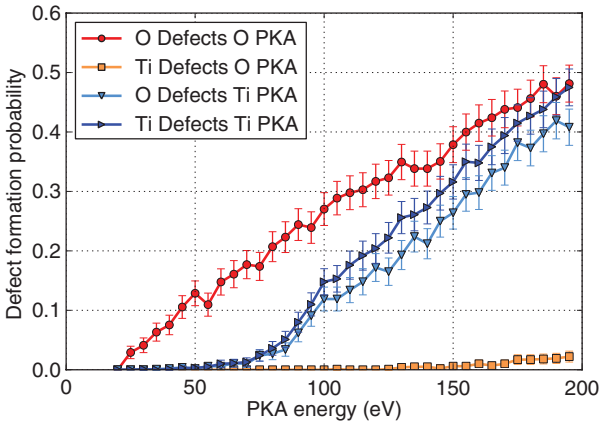

FIG. 9. (Color online) The defect formation probability as a function of PKA energy categorized by species.

which directly associates PKA displacement to Frenkel pair formation.

Another possible definition of E_d relates to the formation of defects on the same sublattice as the PKA. Figure 9 shows the defect formation probability categorized by species of the defect and the PKA species. The important point to note from this figure is that the Ti PKA produces defects on both sublattices at the same value of E_d. As a consequence, the value of E_d for Ti employing a definition based upon the sublattice is equivalent to the more general definition based on Frenkel pairs of any type. This result however, is fortuitous to an extent, since it is conceivable that O defects due to a Ti PKA could have had a threshold lower than that for Ti defects. In this case values of E_d for the Ti PKA would have been dependent on the definition.

D. Comparison with experiment

Comparing the values of E_d calculated in this study to experimental work, the value of E_d calculated for O ($\sim$19 eV) is lower than experimental values in rutile and other ceramic oxides (30 to 50 eV). Two main factors contribute to this discrepancy; the ability to detect the exact onset of defect formation and the difference in time scales between the creation and detection of defects. First, it is clear that the majority of experimental methods require a certain concentration of defects before detection is possible. This reflects the tolerances and background interference inherent in experimental techniques. In contrast, the results presented here have pinpointed the moment a single Frenkel pair was created, which may only be a few simulations out of the thousands carried out.

With regard to the time scales, in the simulations a defect is declared after 10 ps, a much shorter time scale than is possible in experimental procedures. This difference is significant at low PKA energies where localized point defects may be produced that could recombine after the simulated 10 ps but within time scale achieved experimentally. For example, the TRCS work of Smith *et al.*[11–13,30] involved a 25-ns time delay between the electron pulse and the measured anion vacancies. During this period of time, there is an increased likelihood of

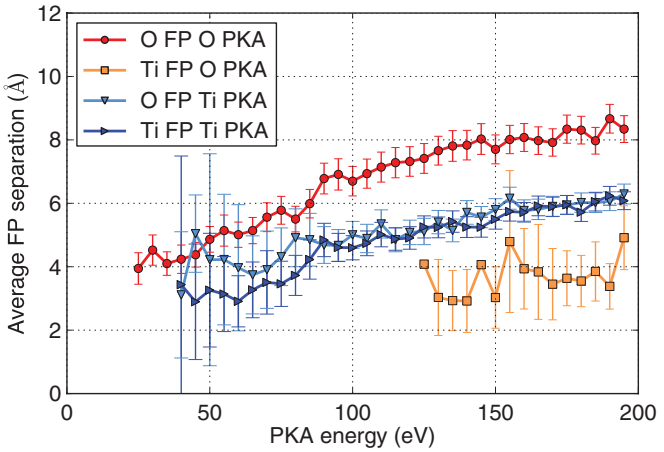

FIG. 10. (Color online) Average Frenkel pair separation per species as a function of PKA energy.

Frenkel pair recombination of close vacancy-interstitial pairs due to local heating. To quantify this, the average Frenkel pair separation was calculated as a function of PKA energy and is shown in Fig. 10. The data here correlates well with the quantities of defects calculated previously in Fig. 9. From the Ti PKA, the equal quantities of Ti and O Frenkel pairs produced are separated by similar distances as PKA energy increases from approximately 5.0 Å at 100 eV to around 6.5 Å at 200 eV. At lower Ti PKA energies around E_d (70 eV), results are inadequate due to the small quantities of defects produced in this region. As there are few Ti defects created from the O PKA, only information regarding the separation of O defects can be extracted. At the value of E_d for O and up to around 50 eV, the O Frenkel pairs are separated by less than 5 Å. The reported high mobility of defects on the O sublattice in oxide ceramics[57–59] along with the heating from the collision cascade suggest recombination of these Frenkel pairs within the time scales of experiments is possible. As PKA energy increases, FP separation increases to around 8 Å at 200 eV. This relates to the inability of the O PKAs to displace the Ti atoms, which results in all the impact kinetic energy being dissipated through the O sublattice.

It must also be noted that differences between experiment and simulation are accentuated by the slow rate of increase in DFP as PKA energy increases. The larger the region in which defect formation is probabilistic, the more difficult it becomes to directly compare results to experiment.

In addition to comparing results to experimental studies, data gathered here may aid future experimental techniques. In particular, experimental procedures such as TRCS that are limited to determining E_d for O. These methods assume that O vacancies are solely attributed to O displacements and therefore once the threshold is reached, the procedure is stopped. However, in this work we find that an equal proportion of Ti and O defects are created from the Ti PKA, as in Fig. 9. This suggests that as incident electron beam energy is increased, two peaks of intensity should be observed. These peaks relate firstly to the O threshold, which creates predominantly O defects and then secondly as the Ti threshold is met due to the O vacancies created by the secondary collisions from Ti displacements. In the work of Smith *et al.*, the first peak was reported at a beam energy of 0.26 MeV, relating to the O vacancies created by O PKAs at around 46 eV. A value of 46 eV corresponds to an DFP of 10% in this work. For a Ti PKA to attain a 10% DFP, an energy of 89 eV is required (see Fig. 7). To achieve an energy transfer of 89 eV to a Ti atom requires a beam energy of at least 1.0 MeV. However, the experimental work of Smith *et al.* using the TRCS methodology only reaches an energy of 0.6 MeV.[11–13,30] Taking the minimum value of E_d for Ti at the onset of defect formation (i.e., 69 eV) the beam energy would still need to be at least 0.82 MeV. This secondary threshold is worthy of consideration in the design of future experiments and would provide an opportunity to observe cation-related processes.

E. The role of the oxygen sublattice

The large FP separations for O seen in Fig. 10 are at first surprising given the low probability of creating a defect. For example at 100 eV the DFP for O is 25% and yet the average FP separation is around 7 Å. One of the main mechanisms responsible for this behavior are replacement chains on the O sublattice. Consecutive knock-on events, where neighboring O atoms are displaced in a concerted manner, dissipate kinetic energy, producing highly separated Frenkel pairs. The dominance of O replacement chains over Ti can be seen in Fig. 11, which shows the average number of replacements as a function of PKA energy. It is also clear that the number of O replacements observed increases at a constant rate which is proportional to the PKA energy. In contrast, the number of Ti replacements converges to around 2 as PKA energy approaches 200 eV, suggesting long-range Ti replacement chains are unlikely.

Due to the regular creation of replacement chains, it is expected that occasionally the head and tail of the chains will meet, forming a replacement loop. In these instances, the perfect crystal structure is restored and a significant proportion of the PKAs kinetic energy has been dissipated in creating the knock-on displacements. Therefore, the frequency of loop formation will indicate a possible mechanism for the rutile lattice to withstand defect formation. The probability of forming a replacement loop is plotted in Fig. 12 as a function

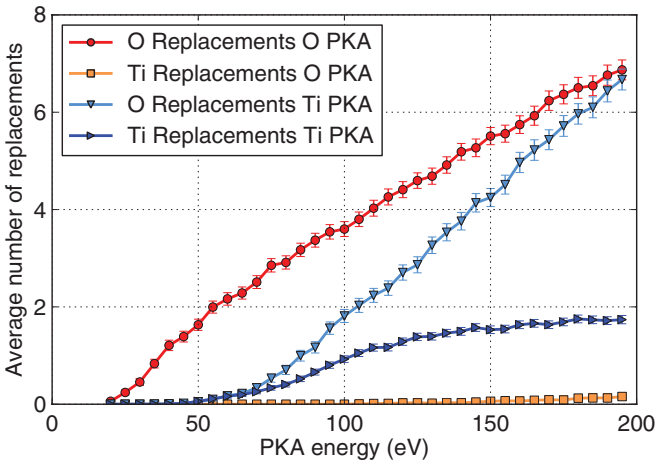

FIG. 11. (Color online) Average number of replacements per species as a function of PKA energy.

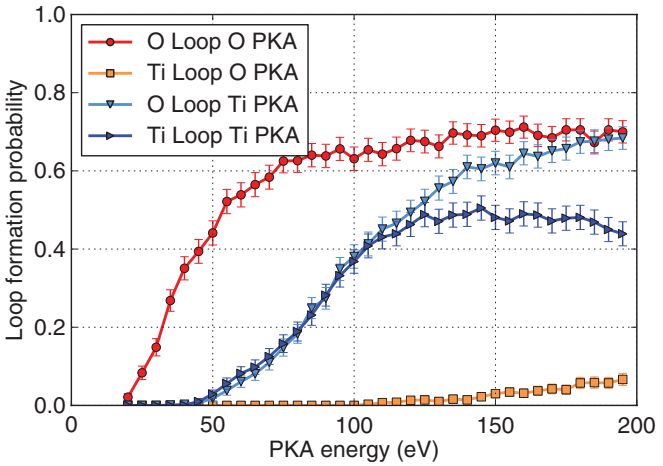

FIG. 12. (Color online) Average loop formation probability as a function of PKA energy for each PKA species.

of PKA energy for both PKA species. An important result here is the sharp increase in the probability of creating loops at low PKA energies, close to the values of E_d. For example, the O PKA which requires around 45 eV to achieve 10% probability of forming an O defect, has a 40% chance of forming an O replacement loop at the same energy. This is also true for the Ti PKA, with loop formation probability higher than the DFP across the complete range of PKA energies. An interesting observation here is the convergence of loop formation probability for the O loops after around 100 eV for the O PKA and also for the Ti PKA at the end of the PKA energy range. Above these energies, the probability of loop formation saturates to a value of around 70%. One explanation for this behavior is that as PKA energy increases, the replacement chains become too long to create a closed loop. At low PKA energies replacement chains created are localized, with the strain from the initial vacancy at the tail of the chain having significant effect on the interstitial created at the head. At larger PKA energies, the effect of the vacancy is minimal to the distant interstitial, with the only occasions of loop formation resulting from secondary, smaller replacement chains.

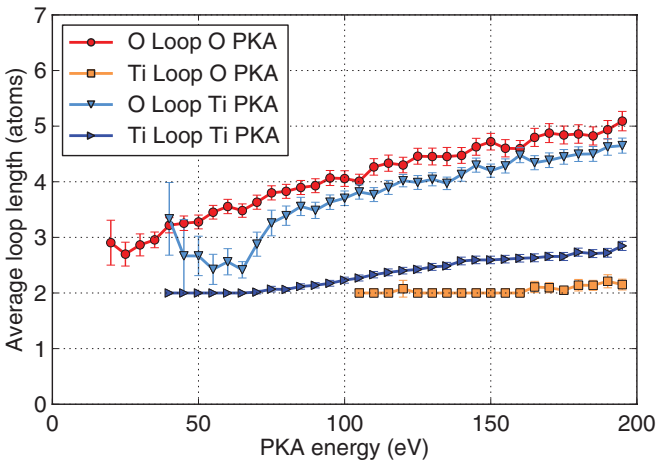

FIG. 13. (Color online) Average length of replacement loops as a function of PKA energy for each PKA species.

Comparisons of the length of the Ti and O replacement loops (Fig. 13) again indicate high activity on the O sublattice. It is apparent that Ti loops are much smaller than O loops, converging to a length of around 2–3 corresponding to simple nearest neighbor exchanges. This supports the ideas taken from Fig. 11 that long-range Ti chains are unlikely at the energies studied. In contrast, O loops average above 2 at low energies, increasing to around 5 at 200 eV. These are remarkably long chains, again indicating the ability of the O sublattice to dissipate the PKA energy through lattice displacements. The difference observed here between the Ti and O replacements chains and loops may help explain the crossover of DFP observed for the Ti and O PKA (Fig. 7). As the O PKA almost solely displaces O atoms, forming O replacement chains, it can take advantage of the high probability of forming loops as PKA energy increases. This reduces the rate at which defects are formed and provides an intuitive explanation of the differences observed in Fig. 8. For the Ti PKA, the inability to form long chains or loops results in a steep rise in DFP once E_d is met.

V. CONCLUSION

Threshold displacement energies E_d in rutile have been systematically calculated using a generalized approach, which is applicable to any crystal structure. Extensive statistics have allowed the definition of defect formation probability as a function of primary knock-on atom (PKA) energy and have given direct insights into defect formation mechanisms at energies around E_d. We find that a probabilistic definition of E_d best describes defect formation, in contrast to the definition used in binary collision packages such as SRIM where a discrete threshold is implicitly implied.

This study has highlighted possible extensions for experimental procedures, in particular methods that involve detection of anion vacancies. The defect production mechanisms observed indicate that the energy at which O defects are created by O displacements is significantly different to the energy at which O defects are created by secondary collisions from Ti displacements. Critically, O defects are created at both the O and Ti threshold displacement energy, suggesting that experimental techniques based on detection of anion vacancies will be able to extrapolate the value of E_d for both atomic species.

O is found to have a lower value of E_d (19 eV) than Ti (69 eV), yet as PKA energy increases the probability of forming Frenkel pairs (FPs) from Ti PKAs becomes greater than from O PKAs. This was found to directly relate to the contrasting behavior observed on the two sublattices. Chains of atomic replacements on the O sublattice were readily created. These chains dissipate the impact kinetic energy whilst maintaining the underlying crystal lattice, producing dispersed and relatively isolated FPs. In contrast, the Ti sublattice was less susceptible to the creation of long replacement chains, with localized nearest neighbor replacements common. Replacement chains were also observed to form loops where the total PKA energy is spent without defect formation. Collectively, these results suggest the radiation tolerance of rutile is directly related to the role of the O sublattice with respect to the Ti sublattice, which may have implications for other oxide ceramics.

*Corresponding author: marc.robinson@curtin.edu.au

[1] G. H. Kinchin and R. S. Pease, Rep. Prog. Phys. **18**, 1 (1955).
[2] M. J. Norgett, M. T. Robinson, and I. M. Torrens, Nucl. Eng. Des. **33**, 50 (1975).
[3] J. F. Ziegler, M. D. Ziegler, and J. P. Biersack, Nucl. Instrum. Methods Phys. Res. Sect. B **268**, 1818 (2010).
[4] G. P. Pells and D. C. Phillips, J. Nucl. Mater. **80**, 207 (1979).
[5] G. P. Pells and D. Phillips, J. Nucl. Mater. **80**, 215 (1979).
[6] G. P. Pells, Radiat. Eff. Defects Solids **64**, 71 (1982).
[7] G. P. Pells and T. Shikama, J. Nucl. Mater. **123**, 1398 (1984).
[8] G. P. Pells, J. Nucl. Mater. **155**, 67 (1988).
[9] Y. Chen, D. Trueblood, O. Schow, and H. Tohver, J. Phys. C **3**, 2501 (1970).
[10] J. L. Grant, R. Cooper, and J. F. Boas, J. Chem. Phys. **88**, 4158 (1988).
[11] K. L. Smith, R. Cooper, M. Colella, and E. R. Vance, Mater. Res. Soc. Symp. Proc. **663**, 373 (2001).
[12] K. L. Smith, M. Colella, R. Cooper, and E. R. Vance, J. Nucl. Mater. **321**, 19 (2003).
[13] K. L. Smith and N. J. Zaluzec, J. Nucl. Mater. **336**, 261 (2005).
[14] J. M. Meese and D. R. Locker, Solid State Commun. **11**, 1547 (1972).
[15] S. J. Zinkle and C. Kinoshita, J. Nucl. Mater. **251**, 200 (1997).
[16] J. B. Gibson, A. N. Goland, M. Milgram, and G. H. Vineyard, Phys. Rev. **120**, 1229 (1960).
[17] C. Erginsoy, G. H. Vineyard, and A. Englert, Phys. Rev. **133**, A595 (1964).
[18] I. M. Torrens, L. T. Chadderton, and D. V. Morgan, J. Appl. Phys. **37**, 2395 (1966).
[19] L. T. Chadderton and I. M. Torrens, Nature (London) **208** (1965).
[20] I. M. Torrens and L. T. Chadderton, Phys. Rev. **159**, 671 (1967).
[21] L. Malerba, J. Perlado, A. Sánchez-Rubio, I. Pastor, L. Colombo, and T. Diaz de la Rubia, J. Nucl. Mater. **283**, 794 (2000).
[22] J. Perlado, L. Malerba, A. Sanchez-Rubio, and T. Diaz De La Rubia, J. Nucl. Mater. **276**, 235 (2000).
[23] L. Malerba and J. M. Perlado, Phys. Rev. B **65**, 045202 (2002).
[24] K. Nordlund, J. Wallenius, and L. Malerba, Nucl. Instrum. Methods Phys. Res. Sect. B **246**, 322 (2006).
[25] M. Gratzel, Nature **414** (2001).
[26] A. L. Linsebigler, G. Lu, and J. T. Yates, Chem. Rev. **95**, 735 (1995).
[27] W. Zhang, M. Zhang, and Z. Yin, Appl. Phys. B **70**, 261 (2000).
[28] A. M. Ruiz, G. Sakai, A. Cornet, K. Shimanoe, J. R. Morante, and N. Yamazoe, Sens. Actuat. B **93**, 509 (2003).
[29] E. C. Buck, Radiat. Eff. Defects Solids **133**, 141 (1995).
[30] K. Smith, N. Zaluzec, and G. Lumpkin, J. Nucl. Mater. **250**, 36 (1997).
[31] D. D. Richardson, Radiat. Eff. Defects Solids **79**, 75 (1983).
[32] B. Thomas, N. Marks, L. Corrales, and R. Devanathan, Nucl. Instrum. Methods Phys. Res. Sect. B **239**, 191 (2005).
[33] I. T. Todorov and W. Smith, Phil. Trans. R. Soc. A **362**, 1835 (2004).
[34] M. Matsui and M. Akaogi, Mol. Simul. **6**, 239 (1991).
[35] J. F. Ziegler, J. P. Biersack, and U. Littmark, *The Stopping and Range of Ions in Matter* (Pergamon, New York, 1985).
[36] R. Smith, D. Bacorisen, B. P. Uberuaga, K. E. Sickafus, J. A. Ball, and R. W. Grimes, J. Phys. Condens. Matter **17**, 875 (2005).
[37] L. Kittiratanawasin, R. Smith, B. P. Uberuaga, and K. E. Sickafus, Nucl. Instrum. Methods Phys. Res. Sect. B **268**, 2901 (2010).
[38] M. Robinson, S. D. Kenny, R. Smith, and M. T. Storr, Nucl. Instrum. Methods Phys. Res. Sect. B **269**, 2539 (2011).
[39] M. Robinson, S. D. Kenny, R. Smith, M. T. Storr, and E. McGee, Nucl. Instrum. Methods Phys. Res. Sect. B **267**, 2967 (2009).
[40] J. J. Thomson, Philos. Mag. **7**, 237 (1904).
[41] J. J. Thomson, in *The Corpuscular Theory of Matter* (Scribner, New York, 1907), Ch. VI, p. 103.
[42] T. Melnyk, O. Knop, and W. Smith, Can. J. Chem. **55**, 1745 (1977).
[43] N. Ashby and W. E. Brittin, Am. J. Phys. **54**, 776 (1986).
[44] L. Glasser and A. G. Every, J. Phys. A: Math. Gen. **25**, 2473 (1992).
[45] J. R. Edmundson, Acta Crystallogr. Sect. A **49**, 648 (1993).
[46] J. R. Edmundson, Acta Crystallogr. Sect. A **48**, 60 (1992).
[47] A. Pérez-Garrido, M. Ortuño, E. Cuevas, and J. Ruiz, J. Phys. A: Math. Gen. **29**, 1973 (1996).
[48] A. Pérez-Garrido and M. A. Moore, Phys. Rev. B **60**, 15628 (1999).
[49] E. L. Altschuler and A. Pérez-Garrido, Phys. Rev. E **73**, 036108 (2006).
[50] D. J. Wales, Science **285**, 1368 (1999).
[51] D. J. Wales and J. P. K. Doye, J. Chem. Phys. **119**, 12409 (2003).
[52] D. J. Wales and S. Ulker, Phys. Rev. B **74**, 212101 (2006).
[53] D. J. Wales, H. McKay, and E. L. Altschuler, Phys. Rev. B **79**, 224115 (2009).
[54] D. J. Wales and J. P. K. Doye, J. Phys. Chem. A **101**, 5111 (1997).
[55] D. J. Wales, *Cambridge Cluster Database*, [http://www-wales.ch.cam.ac.uk/∼wales/CCD/Thomson/].
[56] W. G. Hoover, Phys. Rev. A **31**, 1695 (1985).
[57] T. Ichinomiya, B. P. Uberuaga, K. E. Sickafus, Y. Nishiura, M. Itakura, Y. Chen, Y. Kaneta, and M. Kinoshita, J. Nucl. Mater. **384**, 315 (2009).
[58] K. Govers, S. Lemehov, M. Hou, and M. Verwerft, J. Nucl. Mater. **395**, 131 (2009).
[59] C. A. Gilbert, S. D. Kenny, R. Smith, and E. Sanville, Phys. Rev. B **76**, 184103 (2007).